Understanding and Modeling AC BTI

Hans Reisinger, Tibor Grasser*, Karsten Ermisch, Heiko Nielen, Wolfgang Gustin, and Christian Schlünder

Infineon Technologies, 85579 Neubiberg, am Campeon 1-12; Germany, phone:+49892349210;
e-mail: Hans.Reisinger@infineon.com
* Institute for Microelectronics, Technical University of Vienna, A-1040 Vienna, Austria

***Abstract*—We present a model for AC NBTI which is based on capture and emission of charges in and out of oxide border traps. Capture and emission time constants of these traps are widely distributed from <μs to >10^5s and have been experimentally determined. The model gives a good quantitative understanding of experimental data from alternating stress / recovery sequences. It also provides a physical understanding of all the special features seen in AC NBTI independently of technology parameters.**

Keywords- AC-stress, NBTI, recovery

I INTRODUCTION

Recently it has been shown that BTI threshold shift and recovery can be understood and modeled from charging and discharging of defects in the oxide [1-4]. These defects are characterized by their - field- and temperature dependent - time constants for charge capture and emission τ_c and τ_e. The nature of these defects is not thoroughly understood yet. However, for given electrical stress and recovery fields there is a very simple mathematical description of each defect, which is just an asymmetric RC-element (see Fig. 1c). A full description of a macroscopic MOSFET (containing thousands of defects) then is equivalent to a 2d spectral density map (see Fig. 1b). We want to stress that in principle this mathematical model is independent of the physical model behind it. This study is exclusively devoted to AC-BTI stress. The importance of AC-NBTI has been recognized some time ago [5, 6, 7]. AC-NBTI is the dominating degradation mechanism for computational CMOS logic [8]. An AC- instead of DC-assessment will lower the degradation by more than a factor 2 and increase lifetimes by a factor in the order of 100 [9]. To exploit these benefits, however, clearly demands a solid understanding of AC BTI. We will show that all the special features seen in AC-BTI, i.e. the dependence on duty-factor, the experimentally absent frequency dependence and the reduced recovery-rate - which have not been understood so far - can be well understood now, independently of the technology and also for Hi-K gate stacks.

This paper contains three more sections: Section II provides a brief description of samples and our AC measurement technique and parameters. In section III we outline the properties of our model. Properties of the single defects are not discussed in this work. Temperature and field dependencies of τ_c and τ_e are treated in [3, 4, 10] . The ΔVT step heights produced by single charged defects and the variability of ΔVT are discussed in [11, 12, 13] . In the main section IV we will give explanations for all the special AC-NBTI features mentioned above.

II SAMPLES AND EXPERIMENT

The data analyzed in this study are production-quality pFETs with plasma nitrided oxides (PNO) around 2nm thick and pFETs with 25nm PNO. Also analyzed have been data from Hi-K FETs taken from the literature [14]. Nitrided gate oxides with a thickness of 2nm have been the topic of numerous studies (see [15] and references therein). An inter-technology comparison of some PNO oxides is shown in [4]. It proves that the properties of PNO's with moderate nitridation are comparable w/o major differences.

In our experiments the threshold voltage *VT* has been measured using a measure-stress-measure sequence and our ultrafast direct *VT*-measurement [15]. It is important for the discussion of data that measuring is synchronized with the AC stress signal and starts right after the completion of a stress cycle with a 1 μs measuring delay. Most of our measurements have been done at a frequency of 100 kHz. At this frequency we have been able to sweep the duty factor from 1% to 99% w/o requiring pulses shorter than 100 ns. Like for DC NBTI the measuring delay is a parameter with has strong influence on the measured data, especially on frequency- and duty factor dependence. When comparing different data from the literature, differences in measuring parameters may be much more important than differences in the sample parameters.

III NBTI MODEL

A. Model principles

As pointed out in [2-4, 10] charging and discharging of defects is ruled by stochastic capture and emission processes. When we average over many defects with the same capture and emission time constants τ_c and τ_e then the average occupancy *P* after "applying" stress or recovery, after a stress time t_S or recovery time t_r , respectively, will be described by the following equations:

$$P(t_s) = P(t_s = 0) \times \left[1 - \exp(-t_s / \tau_c)\right] \quad (1)$$

$$P(t_r) = P(t_r = 0) \times \exp(-t_r / \tau_e) \quad (2)$$

For the sake of simplicity the Fermi distribution function is neglected and assumed to be 1 during stress and 0 during recovery. Note that a given, single defect has only two states, occupied or empty.

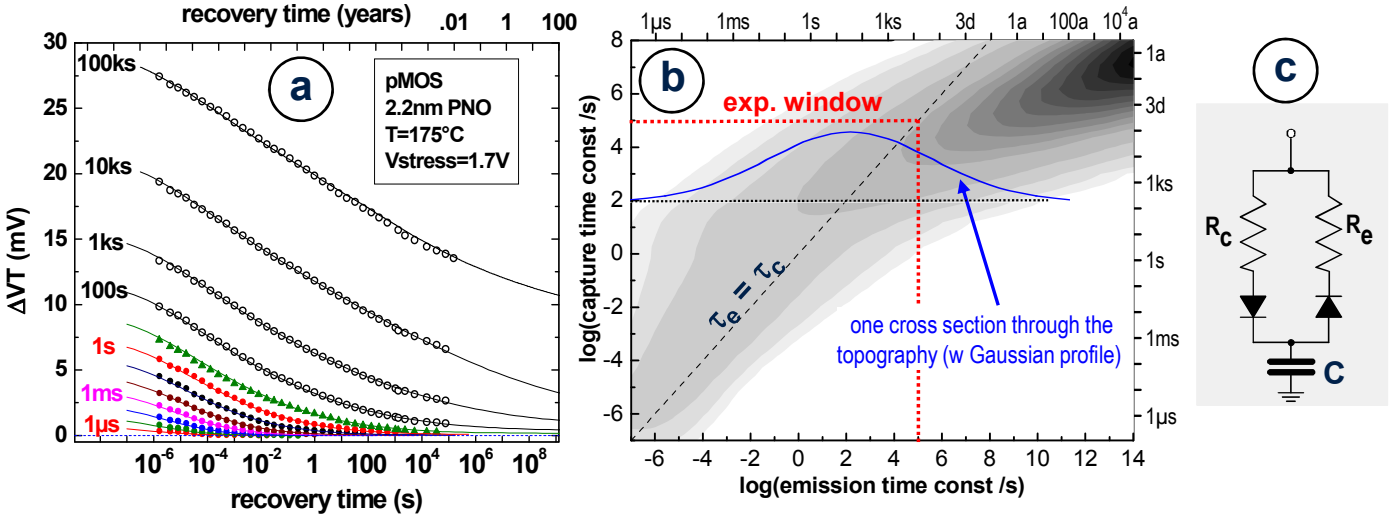

Fig. 1 – **a:** Measured data (symbols) and simulated data (lines) using the spectral density map of Fig. b; labels are denoting the stress times applied consecutively to the sample. **b:** The spectral defect density which has been varied until the best fit in Fig. a has been achieved. The spectral density distribution is parameterized and consists of 10 parameters in total, determining the topography. The spectral density inside the red rectangle is purely experimental, all values covering times $>10^5$s are extrapolations. **c:** Equivalent circuit of a single defect. A single RC-element representing one given defect with capture and emission time constants $\tau_c = CR_c$ and $\tau_e = CR_e$. The RC-element is a 1:1 equivalent to the eq. (1) and (2). The voltage on C corresponds to the ΔVT produced by this defect. A real FET contains a large number of these defects, the individual VTs have to be summed up. Information in Fig. a (time domain) is equivalent to Fig. b (spectral domain).

B. Model Verification

A real FET with a WxL around 0.1x0.5 µm^2 will have a number of ≈500 defects contributing to NBTI degradation (see table 1 in [4] . Clearly to determine the properties of 500 individual defects experimentally is too time consuming to be feasible. Thus a spectral defect density map, taken from the measurement of a very large FET, has to be used instead. In a large FET several thousand defects are active simultaneously. The principles of extracting such a map, of gathering all the information needed, have been outlined in [4] . The extraction method in [4] contains some obvious approximations and is tedious and prone to spurious ΔVT fluctuations. A correct and more straightforward determination of the spectral defect density map is outlined in Fig. 1. Recovery traces are measured covering a regime as wide as possible in stress time as well as in recovery time. Noise and fluctuations in the experimental data should be below a 0.1mV level. Then a defect density map is set up like the one in Fig. 1b. With the complete experimental stress-recovery sequence that has been used for the traces in Fig. 1a this defect density map is then used to re-calculate these traces, resulting in the calculated lines in Fig. 1a. Then, using a nonlinear equation solver, the local density of the defect density map is iteratively varied until a best fit of the calculation (lines) to the experiment (symbols) is achieved. The transformation from the defect density map to the calculated ΔVT curves just employs eq. 1 and 2 for each of the defect classes characterized by their τ_c and τ_e . Each defect class corresponds to a little square in the τ_c / τ_e plane in Fig. 1b. Thus the transformation is trivial, in principle. To avoid any ripple in the calculated data the spacing of the single RC-elements has been chosen to be 0.5 decades. Thus the total number of RC-elements involved in the calculation is in the order of 1000. It is obvious that the information density from the measurement is not high enough to allow the unique determination of 1000 parameters. As a consequence the defect density map in Fig. 1b has been parameterized. Actually a number of 10 parameters is sufficient to describe the topography of the defect density map in Fig. 1b well.

As seen the fit experiment / simulation in Fig. 1a is perfect. This is not a surprise, however. Our model and the way of parameter extraction actually very much resembles a Fourier transformation: A set of data in the time-domain, (example Fig. 1a) is just converted into a set of coefficients in the frequency domain (example Fig. 1b), i.e. the set of "amplitudes" in the 2-dimensional spectral plot. Fig. 1a is quasi a re-conversion into the time-domain. If done correctly, this re-conversion, like a Fourier transformation, exactly reproduces the experimental data as demonstrated in Fig. 1. Of course the model also reproduces the NBTI degradation power-law $\Delta VT(t_s) \propto t^{0.15}$ correctly (not shown). As a further verification and to prove the claim that the model is able to predict recovery and degradation for any *arbitrary* stress-recovery signal sequence, another model verification is shown in Fig. 15 of ref [4]. The agreement between experiment and model is - to our knowledge for the first time - very satisfactory. This proves that the model actually captures all the relevant (capture- and emission-) time constants, from µs to 100ks, and uses them correctly and thus is also valid for AC stress. It is worth mentioning that the model automatically includes any contributions which might be due to a non-recoverable, permanent contribution to NBTI. They are showing up in the right hand side, $\tau_e = 10^{10}$ s to 10^{14} s, of the spectral landscape Fig. 1b and are practically permanent.

IV. AC-NBTI PHENOMENA

In this chapter we will show that the study of the AC-NBTI phenomena will give new insights into some of the NBTI problems. AC-data are easily gained and provide information beyond the DC-NBTI insights. They are more sensitive to extreme tails in the distribution Fig. 1b than DC-NBTI data. We want to stress that any model or theory aiming to explain NBTI (or BTI in general) must be able to explain *all* of the observed AC-BTI phenomena. If a "candidate" for a BTI-theory fails to explain one of these phenomena it just fails to explain BTI at all. We will show that our understanding of AC-NBTI will be able to explain all the special AC-NBTI features. These are the weak frequency dependence, the S-shaped curve of the duty factor dependence, and the AC recovery rate which is initially less than the DC-recovery for short recovery times but has been found to merge the DC recovery curve after long recovery times [14].

Fig. 2 gives an example of the charging of asymmetric RC elements (Fig. 1c), having various τ_c and τ_e values, with a rectangular AC stress signal applied. As seen in Fig. 2 the charging behavior is characterized by a saturation value depending on the duty factor, an envelope charging time constant $\bar{\tau}$ and a value for ripple. A derivation of the charging behavior is straightforward but - to our knowledge - not given in textbooks. The complete derivation will be given in a future publication. We only show the result:

$$(3)\quad V_L(t_{AC}) = \left[1-\exp(-t_{AC}/\bar{\tau}\right]\times\frac{d-du}{1-du}$$

$$V_H(t_{AC}-\Delta T\times(1-\beta)) = \left[1-\exp(-t_{AC}/\bar{\tau}\right]\times\frac{1-u}{1-du}$$

$$with\quad 1/\bar{\tau} = \frac{\beta}{\tau_c}+\frac{1-\beta}{\tau_e}$$

where u and d are abbreviations:

$$u = \exp(-\Delta T\beta/\tau_c)\quad ;\quad d = \exp(-\Delta T(1-\beta)/\tau_e)$$

ΔT is the AC period and t_{AC} is the AC stress time. V_L and V_H are the low- and high levels of the saw tooth function in Fig. 2. $\bar{\tau}$ is the charging time constant seen in Fig. 2, determined by τ_c and τ_e and the duty factor β. Eq.(3) does not contain any approximation. The total computation time for calculating a $V(t_{AC})$ due to AC stress corresponds just to evaluating eq. (3). Done for roughly 1000 defect classes it takes a couple of µs only in total. Thus even for a 10 year stress time at 1 GHz (10^{17} cycles) the calculation is fast. In contrast, calculations based on the reaction / diffusion theory have been reported [16] to consume minutes of computing time only for some 100 stress cycles.

A qualitative and semi-quantitative understanding of all the AC-NBTI features can be obtained from Figs. 3 and 4. These Figs. show the filling state of defects under AC stress, calculated using eq. (3). They explain how the defect density map is sequentially filled during AC stress and emptied again during a recovery phase. Fig. 3 shows an example for the features of the filling state of the defects after applying AC stress with a frequency f = 1Hz and duty factor β = 99%, for an AC stress time t_{AC} = 100 ks and a subsequent recovery time (= measuring delay) of 1 µs. Fig. 3 also serves as a legend for Fig. 4 and uses the same color code. We will see that it is not necessary to consider a special spectral defect density - like the one in Fig. 1b - in order to understand the characteristic AC NBTI features. It

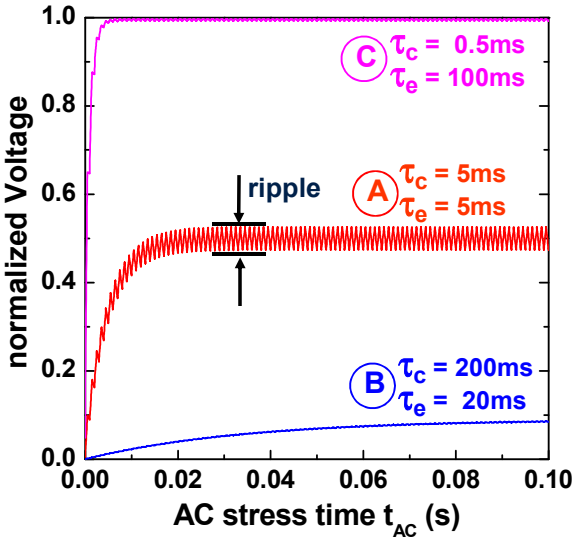

Figure **2:** Some examples of charging curves of RC-elements (=defects) with different charging time constants $\bar{\tau}$ (eq. 3) and different ratios τ_e/τ_c , B=0.1, A=1, C=20. Duty factor is 50% for all curves.

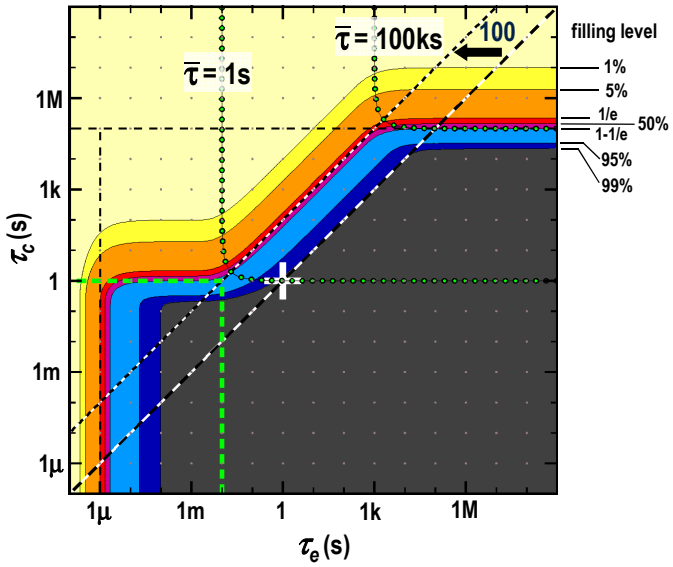

Figure **3:** Occupancy level of defects after AC stress with frequency 1Hz, duty factor 99% (ON/OFF ratio = 100) for a stress time t_{AC} = 100 ks; the status is taken after a full charging cycle with a 1 µs measuring (=recovery) delay. The diagonal line marks $\tau_c = \tau_e$, the shifted diagonal is shifted by a factor 100 corresponding to the ON/OFF ratio. The white cross marks the AC period-time; the green dashed rectangle marks the charging and discharging periods of the AC signal. The dotted green trajectories mark lines of const. charging times $\bar{\tau}$ 1 s and 100 ks. Right hand labels denote the filling state corresponding to the color code. The black horizontal and vertical dash/dotted lines denote the net stress time and the recovery time (= measuring delay), respectively.

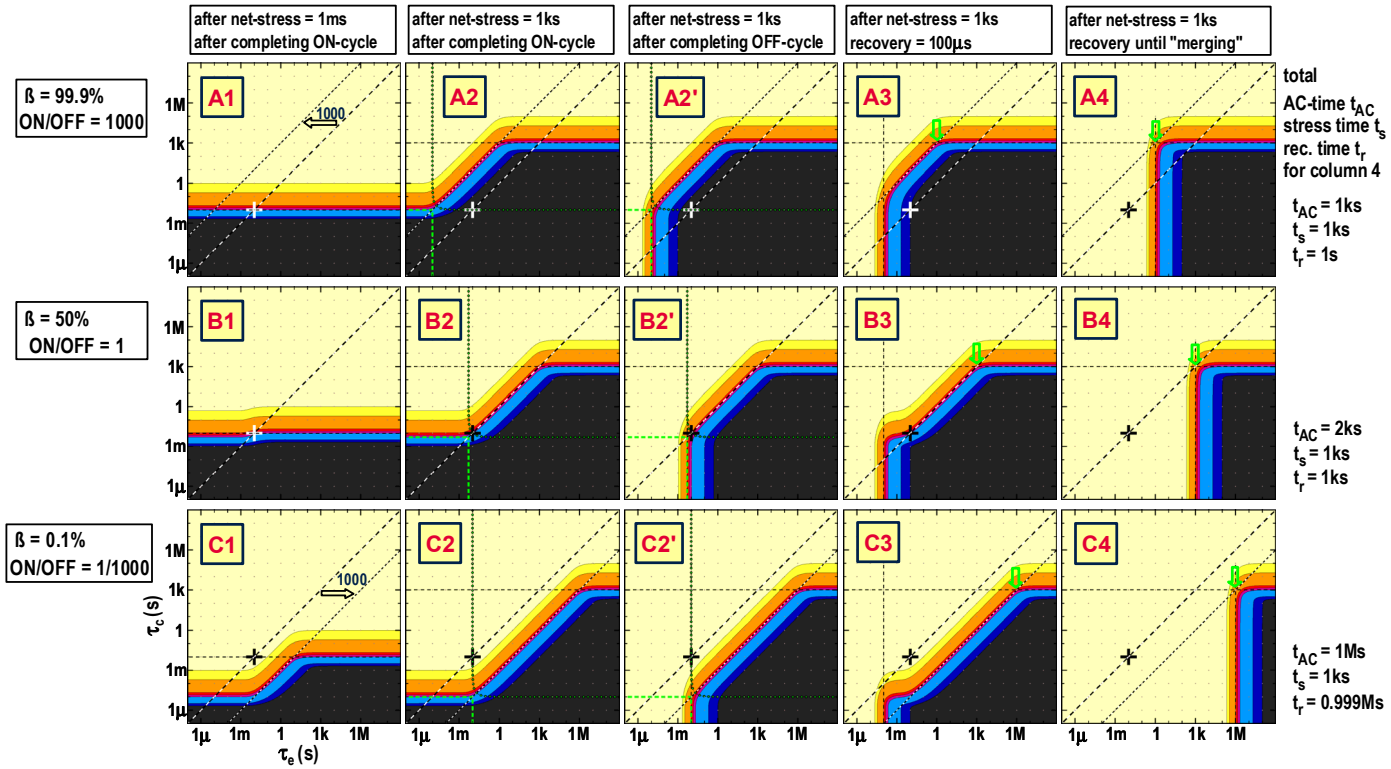

Figure 4. Shows the occupancy levels of RC elements in 3 rows A, B, C with duty factors β from 99.9% to 0.1%. The columns 1 to 4 correspond to different "readout" stress - and recovery times. Columns 2 and 2' show the status just after completing an ON-cycle of the AC signal (w *zero* measuring delay) and after completing an OFF-cycle, respectively. The green arrows mark the intersection of the horizontal τ_c= net-stress-time line and the diagonal $\tau_c = \tau_e * \beta$ which is the point where "merging" of DC and AC recovery occurs. The other symbols and marks are explained in the caption of Fig. 3.

is sufficient to just consider the filling level of the defects in Figs. 3 and 4, which is the same as to assume a "flat" spectral defect density over the τ_e-τ_c plane. Figs. 3 and 4 are, together with eq. (3), almost self explaining. So we give just a description of Figs. 3 and 4 in brief:

- The total area of filled defects in the τ_e-τ_c -plane corresponds to the total charge, i. e. to the value of ΔVT.
- *Under AC stress* the defects fill from bottom to top up to τ_c-levels which can be divided in 3 main regimes:

(I) In regime I the discharging time constant τ_e is *shorter* than the off-time of the AC stress signal; thus all the defects in this regime are completely "reset" during each of the discharging periods of the AC signal; in Fig. 3 this is the regime left of the vertical, green, dashed line marking a τ_e of 10 ms (that is the discharging time of the 1 Hz AC signal with 99% duty factor).

(II) In regime II, located right of regime I, the occupancy level is continuously rising with stress time; only the levels *right* of a diagonal are filled; the filling state is a *linear* function of the ON/OFF ratio and of the ratio τ_e/τ_c ; a filling state of 50% is obtained at the condition $\tau_c/\tau_e <$ ON/OFF (with ON/OFF = β / (1-β))

(III) Regime III is inside the trajectory having a charging time constant $\bar{\tau}$ (eq. 3) equal to the *net stress time* $t_{AC}*\beta$. Defects inside this trajectory (above $\tau_c = t_{AC}*\beta$) remain uncharged or only partly charged.

- *Upon interruption of stress* the charge is "etched" away from left to right to the τ_e-position equal to the actual recovery time t_r. This etching, which is of course independent of the duty factor β, results in a vertical, denuded front (see Figs. 3, 4).
- A *pure DC-stress* without any off periods would fill *full* rectangles instead of a slanted rectangle. Only β = 99.9% is shown in Fig. 4, see Fig. 7 for 100% .
- *Recovery:* The 3 rows in Fig. 4 have different duty factors but receive all the same net-stress-time $t_{AC}*\beta$. Recovery after stress "etches" the bevel anisotropically away from left to right, and the charged shape will eventually become a rectangle. After a certain recovery time t_r *-merge* the "AC-rectangle" and the "DC-rectangle" have equal shapes in good approximation as seen in Fig. 4; this is the point were AC- and DC-recovery traces merge (see Figs. 9, 10). The merging point is marked by green arrows in Fig. 4 and is given by the crossing of the dashed lines. As easily seen this crossing corresponds to the condition $t_r = t_s*(1-\beta)$ (given in labels in the right hand side of Fig. 4).

A. Frequency dependence

It has been shown that over 9 decades in frequency (1Hz to 2 GHz) there is no frequency dependence of the AC-degradation [17]. Fig. 5 shows the experimental curves ΔVT vs. frequency from ref. [17] in comparison with calculated

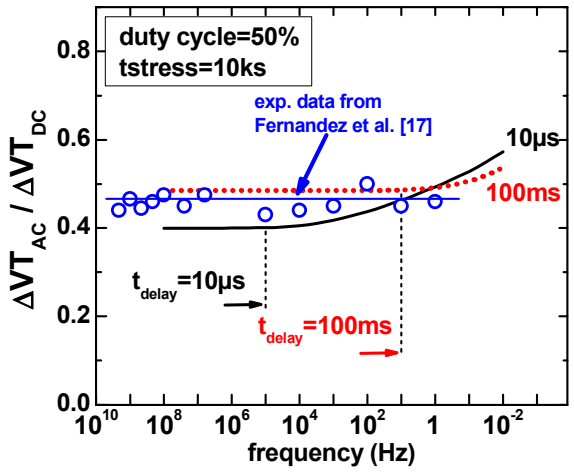

Figure 5: Frequency dependence, calculated with the model parameters from Fig. 1b in comparison with experimental data from ref.[17]. The experimental data were taken with a measuring delay t_D.= 10 s; the calculations have been done with t_D.= 10 us and 100 ms (see right hand labels). The frequency dependence vanishes for frequencies $f > 1/t_D$.

curves for two different measuring delays 10 µs and 100 ms. For the calculated curves a realistic spectral defect density (from Fig. 1b) has been used. It can be seen in Fig. 5 that in the calculated curves the frequency dependence vanishes for frequencies *higher* than the inverse measuring delay $1/t_D$. The reason immediately becomes clear when looking at Fig. 3 : The complete regime *right* of the vertical, dashed green line is "ripple-free". In this regime the AC period $1/f$ (f=1Hz for the case of Fig. 3) is either inside the $\bar{\tau}$=1s trajectory. This means that $1/f$ is shorter than the characteristic charging time $\bar{\tau}$, thus the defect behaves like a low pass filter. Or, in the regime below the $\bar{\tau}$=1s trajectory the occupancy is 100% , which also means zero ripple. Zero ripple is equivalent with zero frequency dependence, so the population in this regime does not change when the frequency changes. The only frequency dependence is found *left* of the dashed, green line. Now, we see in column 3 and 4 of Fig. 4 that the measuring delay t_D *completely erases* the charges left of the green line, and thus erases any frequency dependence for the case that t_D is larger than $1/f$. From Fig. 4 it is obvious that the "charged" area decreases when t_D increases. In contrast in Fig. 5 ΔVT at high frequency the curve for t_D = 100 ms lies significantly higher than the t_D = 10 µs curve. This is just a matter of normalization to the DC degradation. When the measuring delay t_D is kept constant and the frequency f is decreased below $1 / t_D$ then ΔVT is increasing, as seen in Fig. 5. This behavior can be most easily understood looking at Fig. 4 / B3: lowering the frequency moves the black cross upward along the diagonal, thus increasing the area of the rectangular base which is at the bottom of the rising triangle. As a result of this chapter we can say that the missing frequency dependence of NBTI is just due to a measuring artifact. A further obvious result is that the general findings about the frequency dependence are just a matter of the wide distribution of capture and emission time constants and are not dependent on the spectral density. They will be generally valid for any (N)BTI degradation in any technology, also for high-k gate stacks. It should be noted that the apparent frequency-independence does not contain any information about the spectral defect density but is more or less a trivial property.

B. Duty factor dependence

All existing experimental studies about AC-NBTI, e.g. [17, 9] are showing a relation of ΔVT vs. duty cycle having always a typical shape like a lying S. In the vicinity of β = 50% the curve is almost flat. The most prominent and generally observed features are sharp rises in ΔVT between duty factors β=0 and 5% and between 95% and 100%, that is a derivative $\partial \Delta V_T / \partial \beta$ which is very high at the edges of the curve and is close to zero in the middle. The reason for this shape has not yet been convincingly explained. In [4] we could show that a perfect fit of the "S-curve" can be obtained just by summing up the responses of 3 classes of defects, each contributing about an equal amount of ΔVT, and having ratios τ_e / τ_c in the order of 0.001, 1 and 1000. The fast capturing and slowly emitting class with τ_e / τ_c = 0.001 is responsible for the sharp rise between β=0 and 5%. The fast emitting and slowly capturing class with τ_e / τ_c = 1000 is responsible for the sharp rise between β=95% and 100%. The good fit is due to the fact that the shape of the S-curve is mainly determined by the contributions of the defect classes with the *extreme* (low and high) ratios τ_e / τ_c . The assumption of 3 discrete classes contributing is unrealistic, however. So we will do a more general approach in this paper. Fig. 6 shows examples of measured AC-stress data for 3 different PNO thicknesses. Also shown in Fig. 6 are 2 different calculations. One calculation is done by calculating the AC response of a measured DC spectral

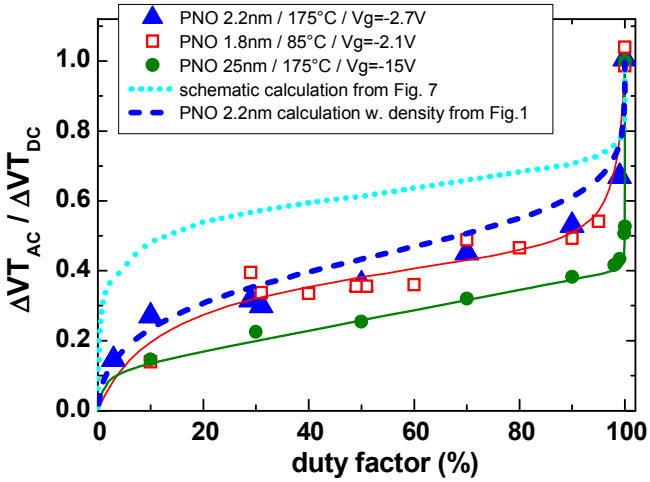

Figure 6. Experimental and calculated curves ΔVT vs duty factor. The calculated curve for the PNO is from the model Fig. 1b and is in fair agreement to experiment. The "schematic" calculation is from an integration over the occupied areas in Fig. 7. All data are for f = 100 kHz and a measuring delay of 1 µs after completion of a stress phase.

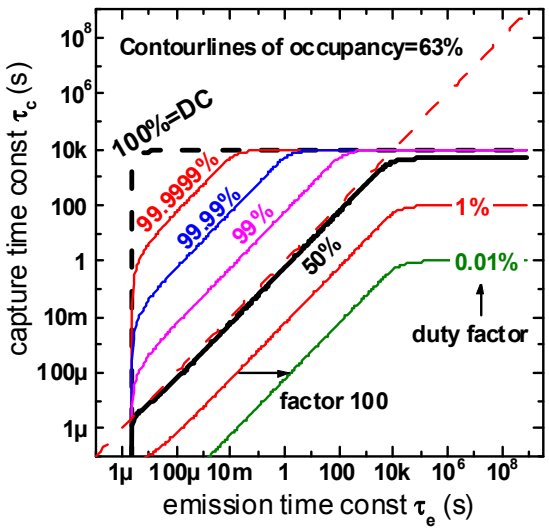

Figure 7. Calculated contour lines of an (1-e) occupancy level in the τ_e-τ_c plane after AC-stress with the duty factor as parameter. Stress frequency is 100 kHz, stress time is 10 ks and measuring delay is 1 µs. For a "flat" spectral defect density the ΔVT corresponds to the area enclosed by the contour lines.

defect density distribution like the one in Fig. 1b, but with stress parameters corresponding to Fig. 6. As seen the fit between calculation and experiment is quite reasonable, though the parameters are coming from a DC measurement. On the other hand even only small contributions of defects having very small or very large ratios τ_e/τ_c , that is defects which are far off the diagonal in Fig. 1b, have a significant influence on the S-curve. The resolution of a DC stress measurements like in Fig. 1 is not sensitive enough to capture these small contributions, though we pushed our measurements to a 0.1mV noise level. Thus a real AC measurement is able to reveal a closer insight into the tails of spectral distribution of defects. Anyway, the fit calculated from the measured DC data is reasonable and can be taken as a proof that our NBTI model is correctly capturing the NBTI physics. In contrast, simulations which have been done using the reaction/diffusion theory, have the characteristic feature that the derivative $\partial\Delta V_T/\partial\beta$ is monotonously decreasing with β [18], which is not in agreement with experiment.

A general understanding of this special derivative $\partial\Delta V_T/\partial\beta$ of AC-NBTI, which is independent of special sample or technology properties, can be drawn from Fig. 7. It shows the calculated contour lines of the charged regimes in the τ_e-τ_c plane, analogously to Fig. 4. The same frequency, measuring delay and stress parameters as for our experimental data have been chosen. The total ΔVT for a duty factor corresponds to the area under the associated contour line in Fig. 7. It becomes obvious from Fig. 7 that this area changes always by roughly the same amount between each of the duty factor steps, for example between 99.9999% and 99.999% or between 1% and 0.1%. Thus it is clear that the derivative $\partial\Delta V_T/\partial\beta$ *must be* diverging close to β = 0% and 100%.

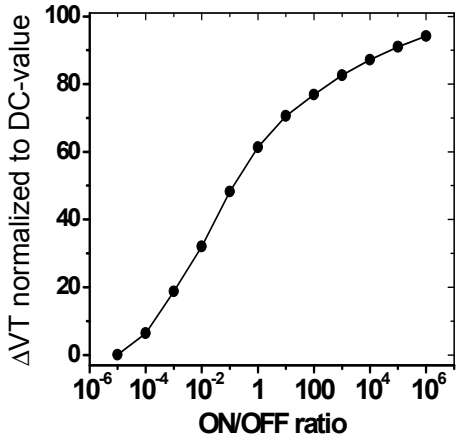

Figure 8. Calculated ΔVT calculated just from integrating over the occupied area in Fig. 7. This curve is identical to the "schematic" curve in Fig. 6. To avoid a divergent integral the area in Fig. 7 has been clipped for values $\tau_e > \tau_e * 10^5$. The transformation from duty factor to ON/OFF ratio converts any S-shaped curves into an almost linear curve and vice versa.

As a consequence it makes sense to *not* plot data against the duty factor but against the ON/OFF ratio $\beta/(1-\beta)$. This transformation from β to the ON/OFF ratio is done in Fig. 8. Fig. 8 shows the area under the contour lines in Fig. 7. The infinite derivatives of the S curve are eliminated, resulting in nearly straight lines. Vice versa, any line being roughly straight when plotted vs. the ON/OFF ratio is transformed into an S shaped curve when plotted against the duty factor. So the shape of the experimental curve can be generally understood w/o even taking special technology or measurement / stress parameters into account.

At this point we want to stress that any conclusions based on all the published curves ΔVT vs. duty factor [9, 17] have to be done with care: The values of the ratios ΔVT(AC) / ΔVT(DC) are strongly influenced by the measuring delay. If the measuring delay is shorter than 1/f then the measured ΔVT is a function of the synchronization of the measurement with the phase of the AC signal. Both these facts have not been considered in any of the "AC-publications" so far.

C. AC recovery

The effect of measuring delay on the measured AC-ΔVT has already been seen qualitatively in Fig. 4. It has been observed experimentally that, compared to the DC value, the AC-ΔVT (cmp. Figs. 4, 6, 7) is reduced even when the duty-factor is only slightly less than 100%, e.g. 99.9%. This is a matter of the "missing triangle" and is self explaining when looking at Figs. 4, 7. It has also been observed experimentally - but not yet been understood - [14] that the AC recovery rate $\partial\Delta V_T/\partial\log(t_r)$ (i) is less than the DC recovery rate, and (ii) that AC and DC recovery traces with the same net stress time as the DC "merge" after a certain recovery time. At this merging point (iii) the initially small AC recovery rate *increases* again. The explanation of the merging of AC- and DC-recovery at a given recovery time has already been explained in Fig. 4. The "merging" occurs

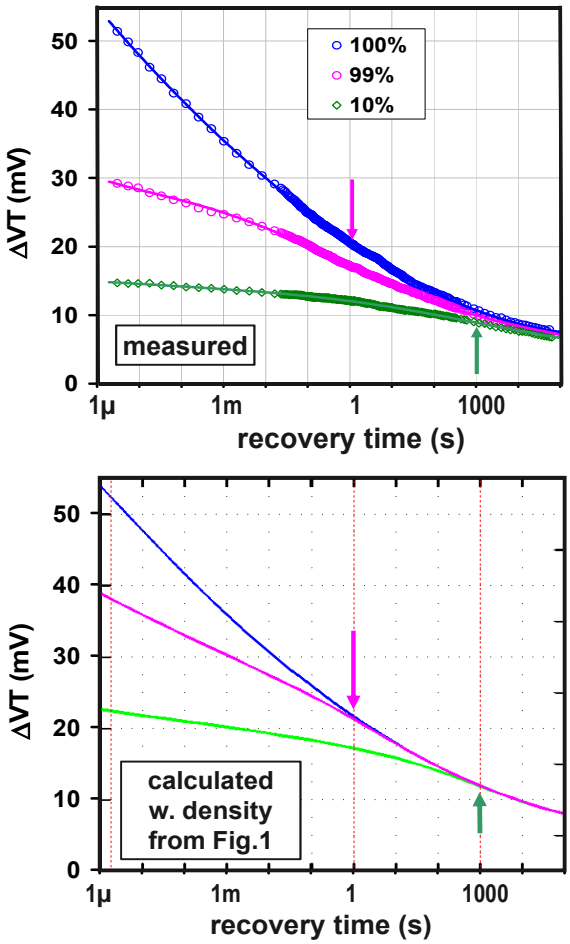

Figure 9 Measured and calculated recovery after stress with duty cycle 100% / 99% / 10%. The corresponding stress times t_{AC} were 100s /101s / 1000s so that the *net stress times* $t_{AC} \times \beta$ are the same for all 3 curves. Arrows mark the points where the AC recovery curves are supposed to merge with the DC curve (cmp. green arrows Fig. 4).

when the AC occupied area in Fig. 4 has "etched" the slanted rectangles from the left down to rectangles. Seen from another point of view, there is almost no short term recovery after AC-stress because this short term recovery has already been anticipated during the stress phase. For example, for the 10% / 1 ks curve in Fig. 9 there have already been 900 s of recovery during the stress phase, prior to the real stress phase. So after a post-stress recovery phase of 1000 s both the 100%-case and the 10% case have "seen" a net stress time of 100 s and a total recovery time of 1000 s and 1900 s, respectively. Note that 1000 s and 1900 s are almost equal on a log time scale. So 1000 s is the point where both recovery curves merge. Fig. 9 and 10 show AC recovery for different duty factors and the same net stress time for our PNO samples and for Hi-K samples from ref [14]. The merging points in Fig. 9 and 10 are marked with arrows. These arrows correspond to the green arrows in Fig. 4. It is clear now that the difference for example between β=100% and β=99% is due to the cut-off edge which is best

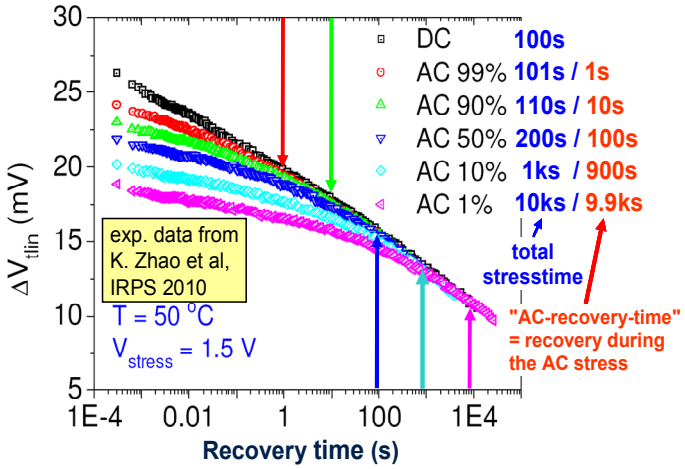

Figure 10. Recovery curves all taken after a net stress time of 100 s with various duty factors. The arrows mark the position were the AC-curves and the DC-curve (100%) are expected to merge.

seen in Fig. 7. The cut-off edge is parallel to the diagonal $\tau_e = \tau_c$. It is clear that, no matter how close β is to 100%, even for 99.99%, there will be an effect. It is noteworthy that - like for the duty factor and frequency dependence -, all considerations about the AC-recovery are independent of the exact spectral distribution of defects and thus are generally valid independent of technology or parameters.

V CONCLUSIONS

The AC NBTI model in this work is based on the analysis of single defects. The conclusions we draw are based on the experimental observations only and do not require further assumptions or models. The new understanding of NBTI leads to a straightforward modeling, especially of AC-NBTI, based on a simple equivalent circuit like in Fig. 1c and a set of empiric parameters. The AC-BTI model provides a physical understanding of all the special AC-NBTI features. This understanding is independent of the technology properties and also valid for high-K and p- and n-MOSFETs. Modeling for practical purposes for any arbitrary stress sequence (DC+AC) requires only short computation times and thus allows implementation into commercial aging tools like Cadence's RelXpert™ [19].

REFERENCES

[1] B. Kaczer, T. Grasser, J. Martin-Martinez, E. Simoen, M. Aoulaiche, Ph. J. Roussel, G. Groeseneken, "NBTI from the perspective of defect states with widely distributed time scales", Proc. IRPS 2009, pp. 55-60.

[2] T. Grasser, H. Reisinger, W. Goes, T. Aichinger, P. Hehenberger, P.-J. Wagner, M. Nelhiebel, J. Franco, B. Kaczer; "Switching oxide traps as the missing link between negative bias temperature instability and random telegraph noise", IEDM technical digest 2009, pp. 729-732.

[3] T. Grasser, H. Reisinger, P.-J. Wagner, F. Schanovsky, W. Goes, B. Kaczer, "The Time Dependent Defect Spectroscopy (TDDS) for the Characterization of the Bias Temperature Instability", proc. IRPS 2010, pp. 26-32.

[4] H. Reisinger, T. Grasser, W. Gustin, and C. Schluender, "The statistical analysis of individual defects constituting NBTI and its implications for modeling DC- and AC-stress", Proc. IRPS 2010, pp. 7-15.

[5] M. A. Alam, "A critical examination of the mechanics of dynamic NBTI for PMOSFETs", IEDM technical digest 2003, pp. 14.4.1-4.

[6] S. Mahapatra P. B. Kumar, and M. A. Alam, "Investigation and Modeling of Interface and Bulk Trap Generation During Negative Bias Temperature Instability of p-MOSFETs", IEEE TED, Vol. 51, No. 9, pp.1371 1379 (2004).

[7] V. Huard, M. Denais, and C. Parthasarathy, "NBTI degradation: From physical mechanisms to modelling", Microelectronics and Reliability, Vol. 46, No. 1, pp. 1-23 (2006).

[8] K. Hofmann, H. Reisinger, K. Ermisch, C. Schluender, W. Gustin, T. Pompl, G. Georgakos, K. v. Arnim, J. Hatsch, T. Kodytek, T. Baumann, .C Pacha, "Highly accurate product-level aging monitoring in 40nm CMOS", Symp. on VLSI Techn. 2010, pp. 27-28.

[9] H. Reisinger, T. Grasser, K. Hofmann, W. Gustin and C. Schluender, "The impact of recovery on BTI reliability assessments", 2010 IIRW final report, pp. 12-16.

[10] T. Grasser, H. Reisinger, P-J. Wagner and B. Kaczer, "Time-dependent defect spectroscopy for characterization of border traps in metal-oxide-semiconductor transistors", Phys. Rev. B, Vol. 82, No. 24, pp. 5318 5327 (2010).

[11] B. Kaczer, Ph. J. Roussel, J. Franco, R. Degraeve, L.-A. Ragnarsson, E. Simoen, G. Groeseneken, T. Grasser, H. Reisinger, "Origin of NBTI variability in deeply scaled pFETs", proc. IRPS 2010. pp. 26-32.

[12] M. F. Bukhori, T. Grasser, B. Kaczer, H. Reisinger, A. Asenov, "'Atomistic' simulation of RTS amplitudes due to single and multiple charged defect states and their Interactions", 2010 IIRW final report, pp.76-79.

[13] M. F. Bukhori, S. Roy, and A Asenov "Simulation of Statistical Aspects of Charge Trapping and Related Degradation in Bulk MOSFETs in the Presence of Random Discrete Dopants", IEEE TED Vol. 57, No. 4, pp. 795-803 (2010).

[14] K. Zhao, J. H. Stathis, A. Kerber and E. Cartier "PBTI Relaxation Dynamics after AC vs. DC Stress in High-K/Metal Gate Stacks" Proc. IRPS 2010, pp. 50-54.

[15] H. Reisinger, O. Blank, W. Heinrigs, W. Gustin, and Ch. Schluender, "A comparison of very fast to very slow components in degradation and recovery due to NBTI and bulk hole trapping to existing physical models", IEEE TDMR, Vol. 7, No. 1, pp. 119-129 (2007).

[16] H. Kufluoglu, V. Reddy, A. Marshall, J. Krick, T. Ragheb, C. Cirba, A. Krishnan, C. Chancellor, "An Extensive and Improved Circuit Simulation Methodology For NBTI Recovery", proc. IRPS 2010, pp. 670-675.

[17] R. Fernandez, B. Kaczer, A. Nackeaerts, R. Rodriguez, M. Nafria, G. Groeseneken, "AC NBTI studied in the 1 Hz - 2 GHz range on dedicated on-chip CMOS circuits", IEDM technical digest 2006, pp.337-340.

[18] A. Jain, A. E. Islam, M. A. Alam, "A Theoretical Study of Negative Bias Temperature Instability in p-Type NEMFET", Proc. Micro/Nano Symposium (UGIM), 2010 , pp. 1-3.

[19] "Reliability Simulation in Integrated Circuit Design - a white paper."[Online Available]: http://www.cadence.com